Title
Solvent Mediated Excited State Proton Transfer in Indigo Carmine

Journal
The Journal of Physical Chemistry Letters, 11(10)

ISSN
1948-7185

Authors
Roy, Partha Pratim
Shee, James
Arsenault, Eric A
et al.

Publication Date
2020-05-21

DOI
10.1021/acs.jpclett.0c00946

Peer reviewed

Solvent Mediated Excited State Proton Transfer in Indigo Carmine

Partha Pratim Roy, James Shee, Eric A. Arsenault, Yusuke Yoneda, Katelyn Feuling, Martin Head-Gordon, and Graham R. Fleming*

ABSTRACT: Excited state proton transfer (ESPT) is thought to be responsible for the photostability of biological molecules, including DNA and proteins, and natural dyes such as indigo. However, the mechanistic role of the solvent interaction in driving ESPT is not well understood. Here, the electronic excited state deactivation dynamics of indigo carmine (InC) is mapped by visible pump−infrared probe and two-dimensional electronic−vibrational (2DEV) spectroscopy and complemented by electronic structure calculations. The observed dynamics reveal notable differences between InC in a protic solvent, D_2O, and an aprotic solvent, deuterated dimethyl sulfoxide (dDMSO). Notably, an acceleration in the excited state decay is observed in D_2O (<10 ps) compared to dDMSO (130 ps). Our data reveals clear evidence for ESPT in D_2O accompanied by a significant change in dipole moment, which is found not to occur in dDMSO. We conclude that the ability of protic solvents to form intermolecular H-bonds with InC enables ESPT, which facilitates a rapid nonradiative $S_1 \rightarrow S_0$ transition via the monoenol intermediate.

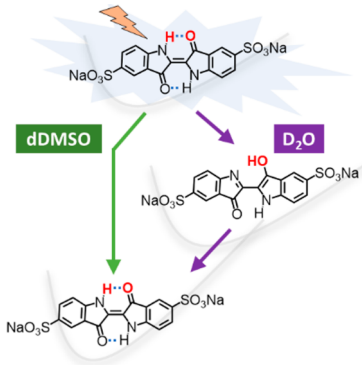

Excited state proton transfer (ESPT) plays a crucial role in the photoprotective mechanism of commercial organic photostabilizers and natural dyes as well as biological molecules such as DNA and proteins.[1−7] Indigo is one such natural dye molecule, which is known for its exceptional photostability.[8,9] Early studies proposed that this is due to intramolecular H-bonding in the excited state, which "locks" the structure in the *trans*-configuration.[10] However, whether or not a proton-transfer reaction takes place to open up a rapid nonradiative pathway to the ground state has remained a subject of controversy.[10−15] Recently, experimental evidence of a rapid (<1 ps) ESPT in indigo carmine (InC) has been reported.[14,16] A solvent-dependent transient spectroscopic study on InC refined this picture, revealing that the dynamics are accelerated in polar protic solvents.[17] Nagasawa et al. proposed that intermolecular H-bonding with the solvent molecule is more effective than intramolecular H-bonding in accelerating the deactivation process. However, none of the studies to date clarify the intricate relationship between solvent−solute interaction and the ESPT.

Two-dimensional electronic−vibrational (2DEV) spectroscopy has several capabilities that can clarify the excited state dynamics of the soluble form of indigo, InC. Namely, the ability to simultaneously observe the electronic and nuclear evolution clarifies on which potential surfaces specific dynamics occur.[18−22] The center line slope (CLS) feature of the 2DEV spectra[23,24] is also a unique quantity that is highly sensitive to changes in electronic structure.[20,25] In this work, we employ visible pump−infrared probe and 2DEV spectroscopy along with electronic structure calculations to make a comparison of the ultrafast excited state dynamics of InC in two different solvents, deuterated dimethyl sulfoxide (dDMSO) and D_2O, each having different polarities and H-bonding abilities, and explore the mechanistic role of system−bath coupling in tuning the excited state deactivation. For InC in D_2O, the CLS provides a clear marker for the structural change accompanying the keto to enol transition, corroborated by electronic structure calculations monitoring changes in the dipole moment.

The primary influence of differential solvent interactions is observed in the ground state FTIR spectra of InC (Figure 1a). In dDMSO, two peaks are observed at 1610 and 1642 cm^{-1}. In D_2O, both peaks shift to a higher frequency (1616 and 1645 cm^{-1}), and the vibrational line widths increase. For the UV−vis steady state spectra (Figure S1), a similar spectral blue shift and broadening are observed in D_2O compared to dDMSO.

A set of visible pump−infrared probe measurements (see SI for experimental details) covering the spectral range from 1480 to 1660 cm^{-1} were carried out in both solvents. The transient infrared spectra are shown in Figure 1b,c. In dDMSO, three major peaks are observed at all pump−probe delays (Figure 1b). In particular, there are two positive peaks at 1642 and 1610 cm^{-1} corresponding to the ground state bleach (GSB) and one broad negative peak at 1530 cm^{-1} corresponding to the excited state absorption (ESA). The two GSB peaks have

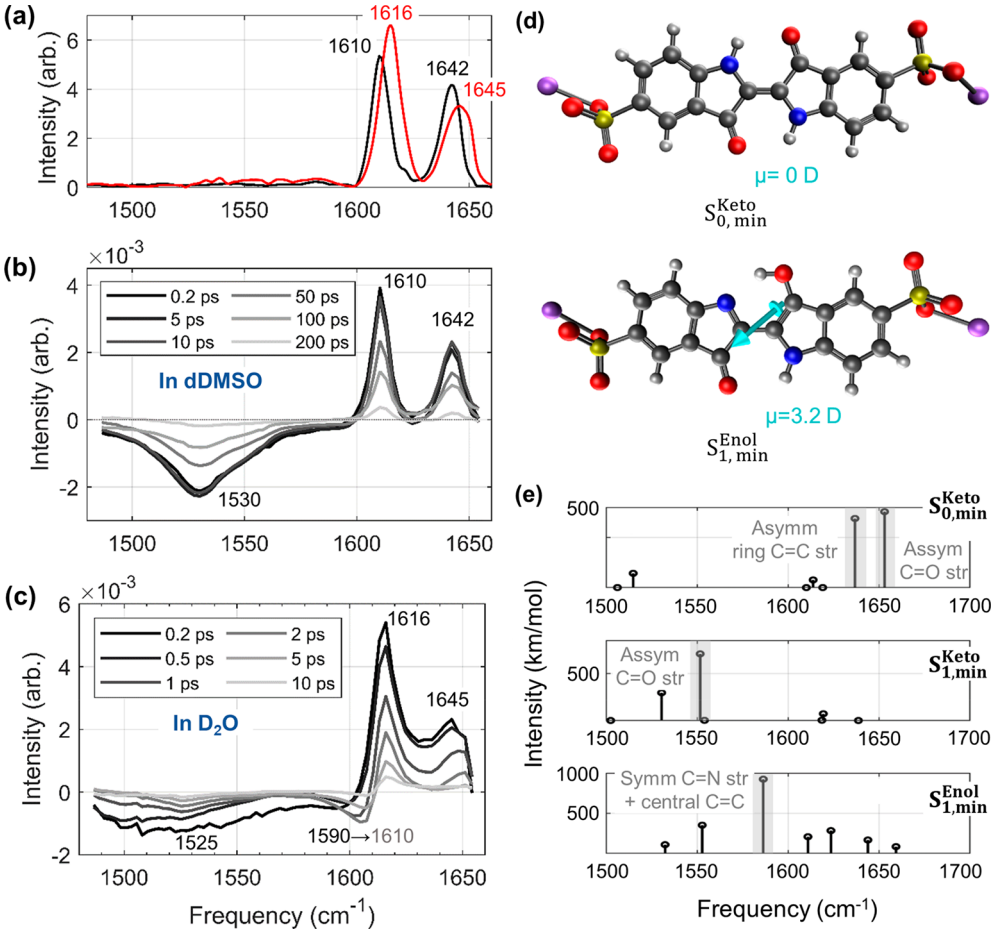

Figure 1. (a) Solvent subtracted ground state FTIR spectra of InC in dDMSO (black) and D_2O (red). Time-resolved infrared spectra of InC in (b) dDMSO and (c) D_2O at different probe delays in the detection frequency range from 1480 to 1660 cm^{-1}, with λ_{exc} = 16 100 cm^{-1}. (d) The calculated the B3LYP/6-31+G* geometries of keto-S_0 and enol-S_1 forms of InC. The overlaid arrow represents the calculated permanent dipole moment. (e) Calculated infrared spectra for the optimized keto-S_0, keto-S_1, and enol-S_1 structures of InC. The major vibrational bands in each graph are highlighted in gray, which match the peaks in the experimental spectra (a–c).

Table 1. Time Constants from Exponential Fits of the Transients at Different Detection Frequencies for InC in dDMSO and D_2O[a]

dDMSO	τ_1 (ps)	D_2O	τ_1 (ps)	τ_2 (ps)	τ_3 (ps)
1642 cm^{-1}	138 ± 10	1645 cm^{-1}	0.62 ± 0.02 (0.8)	5.7 ± 0.7 (0.2)	-
1610 cm^{-1}	120 ± 10	1616 cm^{-1}	0.56 ± 0.02 (0.77)	5.0 ± 0.2 (0.23)	-
1530 cm^{-1}	135 ± 10	1525 cm^{-1}	0.42 ± 0.05 (0.85)	6.0 ± 0.8 (0.15)	-
		1600 cm^{-1}	0.44 ± 0.05 (−0.68)	2.0 ± 0.5 (0.15)	5.7 ± 0.9 (0.17)

[a]See Figures S2–S4. The values in parentheses give the amplitudes associated with each decay component. The negative and positive amplitudes represent exponential rise and decay, respectively.

previously been assigned to the asymmetric stretching of two C=O groups and ring C=C bonds of InC in the ground electronic state (S_0), whereas the ESA peak was assigned to the C=O asymmetric stretching in the excited (S_1) electronic state.[10,26] These assignments agree with our calculated IR spectra (Figure 1e), discussed later. In D_2O, both GSB (1645 and 1616 cm^{-1}) and ESA (1525 cm^{-1}) peaks appear (Figure 1c) at a very similar spectral region as in dDMSO. However, three major contrasts are clearly observed between the evolution of the spectral bands in dDMSO and D_2O (Figure 1b versus 1c). First, a significant acceleration of the kinetics is observed in D_2O compared to dDMSO. It takes about 300 ps for the pump–probe signal to decay to zero in dDMSO and less than 15 ps in D_2O. Second, an additional negative band is found around 1600 cm^{-1} in D_2O, which is completely absent in dDMSO. This 1600 cm^{-1} band is found to be distinct compared to the other three bands in two aspects: (i) this band shows an initial rise (<0.5 ps) followed by an exponential decay, while the other bands show monotonic decay (also see Figures S3 and S4). (ii) a continuous blue shift (1590 → 1610 cm^{-1}) occurred from 0.2 until 1 ps for this particular band, while none of the other bands show any significant transient spectral shift. Third, all three transient bands in dDMSO show a monoexponential decay ($A\exp(-\tau_1/t)$) with a time constant of about 130 ± 20 ps, whereas the corresponding bands in D_2O exhibit a biexponential decay ($A_1\exp(-\tau_1/t) + A_2\exp(-\tau_2/t)$) with time constants of 0.5 ± 0.1 and 6 ± 1 ps (Table 1). The band at 1600 cm^{-1}, however, shows triexponential kinetics

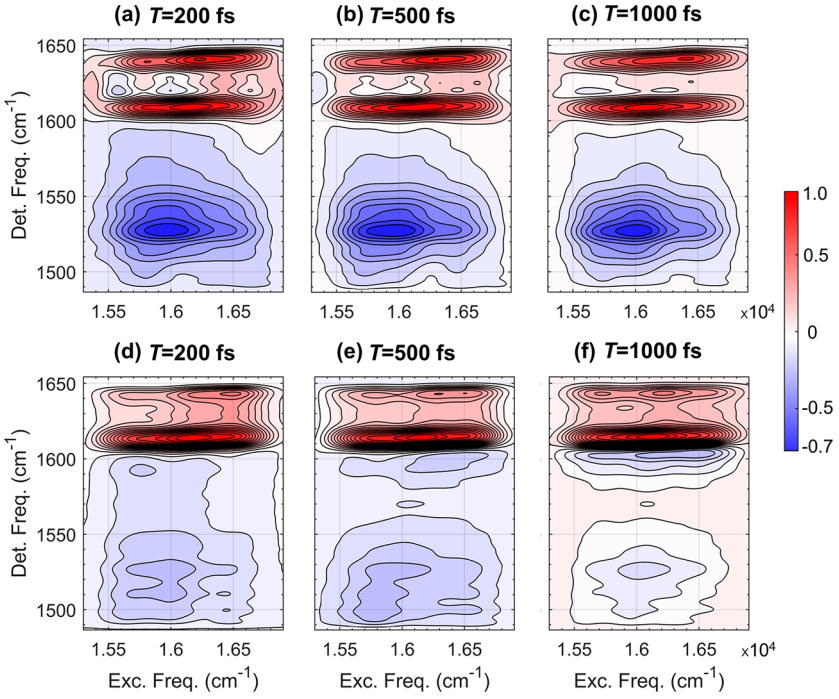

Figure 2. Two-dimensional electronic−vibrational (2DEV) spectra of indigo carmine in (a−c) dDMSO and (d−f) D_2O at different waiting times (T) in the detection frequency range from 1480 to 1660 cm^{-1}, with λ_{exc} = 16 100 cm^{-1}. Each waiting time has been normalized to unity. Contour lines are drawn in 5.2% intervals. The noise floor (3% of the maximum intensity) lies well below the minimum valued contour line.

with one fast rise time constant (0.44 ± 0.05 ps) and two slower decay time constants (2.0 ± 0.5 and 5.7 ± 0.9 ps). The rise time constant of the 1600 cm^{-1} band is nearly the same as the first decay time constants of the other three bands (1645, 1616, and 1530 cm^{-1}) present in D_2O. The biexponential kinetics and the rise of the intermediate band with a rate almost identical to the decay of the other three bands both indicate the formation of an intermediate species during the excited state decay in D_2O, which is absent in dDMSO. The assignment of the intermediate species and the reason behind the blue shift of the 1600 cm^{-1} band will be discussed below.

The involvement of the ESPT has long been discussed in the context of the excited state deactivation mechanism of InC.[12−17] A gas phase *ab initio* calculation of indigo showed that a low-lying conical intersection (CI) between the S_0 and S_1 potential energy surfaces exists for the monoenol isomer.[13] More importantly, the transition from the photoexcited state to the monoenol S_1 minimum was found to correspond to a small energy barrier (~0.2 eV). The barriers to the dienol and *cis*-isomer states appear to be significantly larger, at 1.06 and 1.36 eV, respectively. This suggests that a nonradiative route via the monoenol intermediate is the most favorable pathway for the $S_1 \rightarrow S_0$ transition. With these findings in mind, we performed density functional theory (DFT) calculations to characterize the intermediate band found in our pump−probe spectra. In particular, we utilized the B3LYP functional[27,28] and 6-31+G* basis set[29] with the polarizable continuum model (PCM)[30] (using the Q-Chem 5.2 quantum chemistry package[31]) to compute the minimum energy geometries of keto and monoenol forms on their ground ($S_{0,min}^{Keto}$) and excited ($S_{1,min}^{Keto}$, $S_{1,min}^{Enol}$) potential energy surfaces and the corresponding infrared vibrational frequencies (Figure 1d,e). Excited state optimizations and properties were computed via linear-response time-dependent (TD-) DFT.[32,33]

The calculated IR spectra (Figure 1e) show good agreement with the experimental spectra (Figure 1a−c). Two major peaks (1635 and 1653 cm^{-1}) appear for $S_{0,min}^{Keto}$ and match the ground state FTIR spectra. One major peak (1552 cm^{-1}) for $S_{1,min}^{Keto}$ matches the ESA peak in the pump−probe spectra of InC in both dDMSO (1530 cm^{-1}) and D_2O (1525 cm^{-1}). Most significantly, a strong peak appears at 1585 cm^{-1} for $S_{1,min}^{Enol}$, which characterizes the intermediate band at 1600 cm^{-1} in the pump−probe spectra of InC in D_2O, and is assigned to the symmetric C−N stretch coupled with the central C=C stretch in the enol-S_1 state. This assignment explains the appearance of the intermediate band and subsequent spectral blue shift as follows. As the keto isomer is symmetric (C_{2h}), any symmetric vibrational mode should be Raman active (reported in ref 17) and IR inactive. As soon as the proton transfer is initiated, the symmetry is broken as the keto is converted to the monoenol form and the symmetric vibration becomes IR active. During the process of keto to enol conversion, the C−N bond begins to adopt increasing double bond character, resulting in an increase in vibrational frequency. Furthermore, the survival of the asymmetric C=O stretch ESA band after the ESPT (~0.5 ps) in D_2O (Figure 1c) is consistent with a single proton-transfer mechanism, as suggested earlier,[13] and, in fact, clearly rules out the double proton-transfer mechanism.

The pump−probe results in conjunction with the theoretical calculations provide strong evidence of the proton transferred monoenol species in D_2O and of its absence in dDMSO. To elucidate the picture of the solvent-dependent potential energy landscape, we utilized 2DEV spectroscopy (see SI for experimental details). 2DEV spectra were recorded in dDMSO and D_2O with waiting times varying from 0 to 1 and 1 to 2.2 ps with time steps of 20 and 100 fs, respectively. Figure 2 illustrates typical 2DEV spectra at three different waiting times, T = 200, 500, and 1000 fs. The GSB (positive)

and ESA (negative) bands are illustrated by red and blue colors, respectively. The appearance of the 2DEV spectral bands in both dDMSO and D_2O are the same as the pump–probe spectra shown earlier (Figure 1b,c), because 2DEV is just the two-dimensional analog of the former technique.

2DEV spectroscopy provides new information about the correlation of nuclear and electronic degrees of freedom in the form of the center line slope (CLS).[24,34] The dephasing of the vibrational modes and a change of the molecular electronic structure manifest as dynamical changes in the CLS of 2DEV bands. Furthermore, the magnitude of the CLS gives a direct estimation of the relative strength of the vibrational coupling of the solvent bath with the electronic excited state versus the ground state. The CLSs are calculated by the method of conditional averaging described in detail in ref 25. Here, the slope has been calculated along the excitation frequency axis (ω_{vis}), though the same dynamical information could be obtained by calculating the CLS along the detection frequency axis (ω_{IR}).[23] The spectral region with an amplitude within 25–50% of the peak maximum (to exclude any noise or peak overlap effects) is chosen when calculating the CLS. For each spectral band, the CLS is plotted as a function of waiting time (Figure 3). Both in dDMSO and D_2O, the GSB bands (1642,

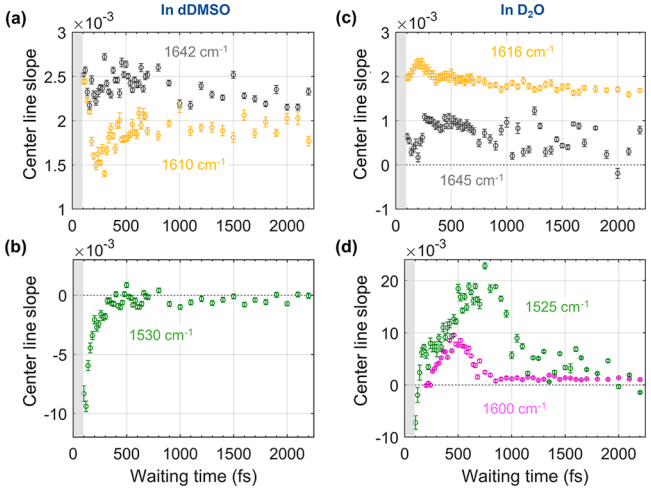

Figure 3. Center line slope (CLS) of different vibrational bands along the excitation axis as a function of waiting time (T) for InC in (a,b) dDMSO and (c,d) D_2O. In (a,c), the black and yellow points represent the CLS dynamics for the specified GSB bands, whereas in (b,d), the green and magenta points represent the CLS dynamics for the specified ESA bands. In each graph, the circles represent the experimental data points, and the vertical bar represents the corresponding standard error. The gray shaded area covers the region that falls within time resolution of the experiment.

1610 cm^{-1} in dDMSO and 1645, 1616 cm^{-1} in D_2O) show no significant change through the waiting time (Figure 3a,c), whereas the ESA bands (1530 cm^{-1} in dDMSO and 1525, 1600 cm^{-1} in D_2O) start with a large negative slope and show a substantial change with increased waiting time (Figure 3b,d). This indicates a stronger coupling of the solvent environment with the electronic excited state (S_1) of InC compared to its electronic ground state, which agrees with the work of Nagasawa et al.[17] More significantly, a striking difference between the CLS dynamics of these ESA bands in dDMSO and D_2O is observed. The CLS of the 1530 cm^{-1} band in dDMSO shows only a rapid ($\tau = 90 \pm 20$ fs) exponential decay (Figure 3b), consistent with a simple vibrational dephasing model.[23] In D_2O, the CLS of the 1525 cm^{-1} band also shows a sharp decay initially but later (~200 fs) flips sign from negative to positive, which is followed by a decay to zero within 2 ps (Figure 3d). The 1600 cm^{-1} band follows the same trend following its appearance around T = 200 fs.

The stark contrast in the CLS plots of the ESA bands in dDMSO and D_2O clearly demonstrates different evolution of the electronic and nuclear degrees of freedom of InC in these two solvents. The sign flip of the CLS corresponds to a switch in the correlation between ω_{vis} and ω_{IR}. The change in correlation is directly linked to the change in the permanent dipole of the molecule and its consequent effect on the solvent.[25] When the system has zero dipole moment, the surrounding polar solvent molecules are arranged without any specific orientations. As soon as the system adopts a nonzero dipole, the libration of the solvent molecules will stabilize the system and create a correlation between ω_{vis} and ω_{IR}. When the direction of dipole moment flips by >90°, the stabilizing solvent environment becomes destabilizing and the correlation between ω_{vis} and ω_{IR} switches its sign. We tracked the change in molecular dipole moment from $S_{1,FC}^{Keto}$ (Franck–Condon region) → $S_{1,min}^{Keto}$ → $S_{1,min}^{Enol}$ → enol S_0/S_1 minimum energy crossing point (MECP) to explain the corresponding change in the CLS. For the first three states, we utilized the same level of theory used for the vibrational frequency calculations, i.e., B3LYP/6-31+G* with the PCM solvation treatment. We believe this level of theory provides an accurate description, in light of the good agreement of the calculated vertical excitation energy (2.11 eV) with the experimental value (1.99 eV), however, the lack of explicit solvent cannot properly describe the effects of solute–solvent intermolecular H-bonding. Optimization of the geometry at the MECP between enol S_0 and S_1 potential energy surfaces was performed via the branching plane algorithm[35,36] and required use of the spin–flip variant of time-dependent density functional theory (SF-TDDFT),[37] which describes the S_0 and S_1 states on an equal footing, i.e., as excitations from a shared triplet reference state (a crucial property as their energies approach degeneracy). All SF-TDDFT calculations utilize the BHHLYP functional.[38,39] While conformations defined by rotation of the SO_3Na end groups were found to be nearly energetically degenerate (we found a range of merely 0.06 kcal/mol), the associated permanent dipole moments varied substantially (from 0 to ~18 D). However, as the end groups are not expected to significantly affect the photophysical properties of InC (indeed, the calculated relative energetics of the relevant states along the reaction pathway are indistinguishable with and without end groups, as shown in Tables S1 and S2), in what follows, we analyze the evolution of the dipole moments of the indigo molecule, i.e., InC with end groups removed.

The calculated geometry of the keto-S_1 minimum (Figure S5) is planar and the dipole moments of both InC and indigo are zero. This is inconsistent with the initial (~100 fs) large negative amplitude of the CLS for the ESA band in both solvents (Figure 3b,d). However, in a previous theoretical study of the nonadiabatic dynamics of a truncated version of the indigo molecule, typical trajectories showed a twist of up to 25–30° around the central C=C bond.[12] This twist breaks the symmetry and can induce a permanent dipole in InC, as is known to occur, for example, in ethylene upon photoexcitation to the S_1 state.[40] To investigate this further, we computed the energy and dipole moment of the $S_{1,min}^{Keto}$ state as a function

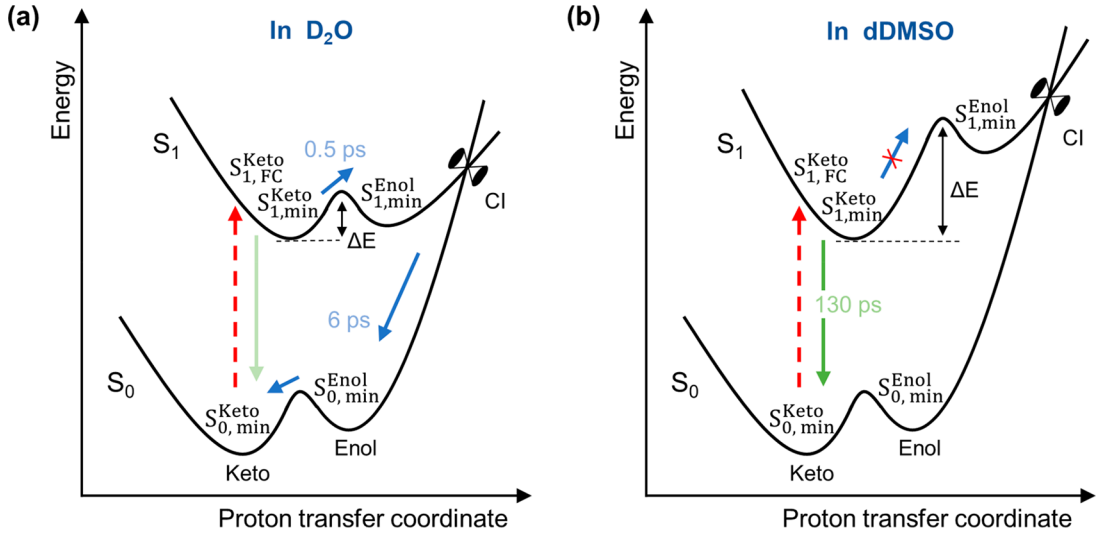

Figure 4. Schematic potential surfaces as a function of proton-transfer reaction coordinate pathways proposed for InC in (a) D_2O and (b) dDMSO, respectively. In each graph, the red dotted arrow represents the photoexcitation, and ΔE represents the energy barrier between keto and enol forms in the S_1 state of InC. The green and blue arrows in both (a,b) represent two different excited state deactivation pathways. The latter is significantly less likely in dDMSO due to a higher energy barrier (ΔE).

of dihedral angle around the central C=C bond, again using indigo as a proxy for InC (Figure S6), which shows that a twist up to ∼15° is easily accessible at room temperature (∼0.6 kcal mol^{-1}/∼0.026 eV) without any other external force. This would give rise to a nonzero permanent dipole (Figure S7), supported by the large initial CLS magnitude, and it is likely that inclusion of explicit intermolecular H-bonding interactions should further stabilize configurations with nonzero dihedral angles.

The optimized geometry and corresponding dipole moment of the monoenol S_1 minimum for InC are shown in Figure 1e. The enol excited state minimum is slightly uphill by ∼0.04 eV from the Franck−Condon keto-S_1 state. This is consistent with a temperature-dependent fluorescence study, which found that the activation energy for the nonradiative deactivation was higher in DMSO (8.8 kJ mol^{-1}/0.091 eV) than in water (3.5 kJ mol^{-1}/ 0.037 eV).[17] The single proton-transfer process involves a change in the dipole moment shown explicitly for indigo in Figure S7, which correlates with the change in sign of the CLS in Figure 3d. The computed geometry at the S_0/S_1 MECP is very similar to that of the enol S_1 minimum, in agreement with calculations from ref 13. Our calculations also show that this MECP is ∼0.5 eV above the enol S_1 minimum state, using SF-TDDFT for both states, and corresponds to a decrease in magnitude of the dipole moment, while its direction remains nearly unchanged (Figure S8). This suggests that back proton transfer occurs after the conical intersection on the ground state potential energy surface, which can be observed in the decay of the CLS of the 1525 and 1600 cm^{-1} modes back to zero after reaching a maximum (Figure 3d).

In summary, both pump−probe and 2DEV results show that the excited state deactivation dynamics of InC is strongly solvent-dependent. In dDMSO, the decay is monoexponential with a time constant of 130 ps matching the excited lifetime (∼110 ps) reported for InC in a similar protic solvent, like dimethylformamide.[15] On the other hand, InC in D_2O shows accelerated biexponential kinetics via a rapid (∼0.5 ps) ESPT process, supported by our *ab initio* calculations. The proton transfer from N−H to the C=O group can be either intramolecular or intermolecular, i.e., "indirectly" via the solvent though the formation of anionic intermediate. However, the lack of evidence of an anionic intermediate species before the S_1-enol formation excludes the latter mechanism. A similar time scale for the intramolecular ESPT (<0.5 ps) in indigo has been suggested by Iwakura et al.,[14,16] although they concluded that the enol to keto back proton transfer occurs in the S_1 state (<1 ps), inconsistent with our interpretation. Our work finds that enol to keto back transfer (∼6 ps) is likely to take place in the S_0 state after passing the conical intersection, in agreement with previous studies by Yamazaki[12] and Cui et al.[13]

The combination of 2DEV CLSs and electronic structure calculations provides a powerful probe of the excited state dynamics via tracking changes in electronic structure and accompanying nuclear rearrangements. Specifically for InC, two distinct excited state deactivation pathways in dDMSO and D_2O are apparent (Figure 4). In a nonprotic solvent such as dDMSO, the barrier to enol formation is high, and the conical intersection region is not reached. However, in D_2O, we find that facile excited state proton transfer makes deactivation through the conical intersection the dominant pathway.

AUTHOR INFORMATION

Corresponding Author

Graham R. Fleming − *Department of Chemistry, University of California, Berkeley, California 94720, United States; Molecular Biophysics and Integrated Bioimaging Division, Lawrence Berkeley National Laboratory, Berkeley, California*

94720, United States; Kavli Energy Nanoscience Institute at Berkeley, Berkeley, California 94720, United States; orcid.org/0000-0003-0847-1838; Phone: +1 510 643 2735; Email: grfleming@lbl.gov

Authors

Partha Pratim Roy − *Department of Chemistry, University of California, Berkeley, California 94720, United States; Molecular Biophysics and Integrated Bioimaging Division, Lawrence Berkeley National Laboratory, Berkeley, California 94720, United States*

James Shee − *Department of Chemistry, Kenneth S. Pitzer Center for Theoretical Chemistry, University of California, Berkeley, California 94720, United States;* orcid.org/0000-0001-8333-8151

Eric A. Arsenault − *Department of Chemistry, University of California, Berkeley, California 94720, United States; Molecular Biophysics and Integrated Bioimaging Division, Lawrence Berkeley National Laboratory, Berkeley, California 94720, United States; Kavli Energy Nanoscience Institute at Berkeley, Berkeley, California 94720, United States*

Yusuke Yoneda − *Department of Chemistry, University of California, Berkeley, California 94720, United States; Molecular Biophysics and Integrated Bioimaging Division, Lawrence Berkeley National Laboratory, Berkeley, California 94720, United States; Kavli Energy Nanoscience Institute at Berkeley, Berkeley, California 94720, United States*

Katelyn Feuling − *Department of Chemistry, University of California, Berkeley, California 94720, United States; Molecular Biophysics and Integrated Bioimaging Division, Lawrence Berkeley National Laboratory, Berkeley, California 94720, United States; Department of Chemistry, University of Minnesota, Minneapolis, Minnesota 55455, United States*

Martin Head-Gordon − *Department of Chemistry, Kenneth S. Pitzer Center for Theoretical Chemistry, University of California, Berkeley, California 94720, United States; Kavli Energy Nanoscience Institute at Berkeley, Berkeley, California 94720, United States;* orcid.org/0000-0002-4309-6669

■ ACKNOWLEDGMENTS

The experimental work (P.P.R., E.A.A., Y.Y., K.F., and G.R.F.) was supported by the U.S. Department of Energy, Office of Science, Basic Energy Sciences, Chemical Sciences, Geosciences, and Biosciences Division to G.R.F. The electronic structure work (M.H.-G. and J.S.) was supported by the Director, Office of Science, Office of Basic Energy Sciences, of the U.S. Department of Energy under Contract No. DE-AC02-05CH11231. E.A.A. acknowledges the support of the Berkeley Fellowship and the National Science Foundation Graduate Research Fellowship (Grant No. DGE 1752814). Y.Y. appreciates the support of the Japan Society for the Promotion of Science (JSPS) Postdoctoral Fellowship for Research Abroad. K.F. appreciates the support of the university of Minnesota Leadership Minor.

■ REFERENCES

(1) Tuna, D.; Došlić, N.; Mališ, M.; Sobolewski, A. L.; Domcke, W. Mechanisms of Photostability in Kynurenines: A Joint Electronic-Structure and Dynamics Study. *J. Phys. Chem. B* **2015**, *119*, 2112−2124.

(2) Perun, S.; Sobolewski, A. L.; Domcke, W. Ab Initio Studies on the Radiationless Decay Mechanisms of the Lowest Excited Singlet States of 9H-Adenine. *J. Am. Chem. Soc.* **2005**, *127*, 6257−6265.

(3) Sobolewski, A. L.; Domcke, W. The Chemical Physics of the Photostability of Life. *Europhys. News* **2006**, *37*, 20−23.

(4) Sobolewski, A. L.; Domcke, W. Relevance of Electron-Driven Proton-Transfer Processes for the Photostability of Proteins. *ChemPhysChem* **2006**, *7*, 561−564.

(5) Sobolewski, A. L.; Domcke, W. Computational Studies of the Photophysics of Hydrogen-Bonded Molecular Systems. *J. Phys. Chem. A* **2007**, *111*, 11725−11735.

(6) Migani, A.; Blancafort, L.; Robb, M. A.; DeBellis, A. D. An Extended Conical Intersection Seam Associated with a Manifold of Decay Paths: Excited-State Intramolecular Proton Transfer in O-Hydroxybenzaldehyde. *J. Am. Chem. Soc.* **2008**, *130*, 6932−6933.

(7) Barbatti, M.; Aquino, A. J. A.; Lischka, H.; Schriever, C.; Lochbrunner, S.; Riedle, E. Ultrafast Internal Conversion Pathway and Mechanism in 2-(2'-Hydroxyphenyl)Benzothiazole: A Case Study for Excited-State Intramolecular Proton Transfer Systems. *Phys. Chem. Chem. Phys.* **2009**, *11*, 1406−1415.

(8) Melo, M. J.; Claro, A. Bright Light: Microspectrofluorimetry for the Characterization of Lake Pigments and Dyes in Works of Art. *Acc. Chem. Res.* **2010**, *43*, 857−866.

(9) Splitstoser, J. C.; Dillehay, T. D.; Wouters, J.; Claro, A. Early Pre-Hispanic Use of Indigo Blue in Peru. *Sci. Adv.* **2016**, *2*, e1501623.

(10) Elsaesser, T.; Kaiser, W.; Lüttke, W. Picosecond Spectroscopy of Intramolecular Hydrogen Bonds in 4,4',7,7'-Tetramethylindigo. *J. Phys. Chem.* **1986**, *90*, 2901−2905.

(11) Bernardino, N. D.; Brown-Xu, S.; Gustafson, T. L.; De Faria, D. L. A. Time-Resolved Spectroscopy of Indigo and of a Maya Blue Simulant. *J. Phys. Chem. C* **2016**, *120*, 21905−21914.

(12) Cui, G.; Thiel, W. Nonadiabatic Dynamics of a Truncated Indigo Model. *Phys. Chem. Chem. Phys.* **2012**, *14*, 12378−12384.

(13) Yamazaki, S.; Sobolewski, A. L.; Domcke, W. Molecular Mechanisms of the Photostability of Indigo. *Phys. Chem. Chem. Phys.* **2011**, *13*, 1618−1628.

(14) Iwakura, I.; Yabushita, A.; Kobayashi, T. Why Is Indigo Photostable over Extremely Long Periods? *Chem. Lett.* **2009**, *38*, 1020.

(15) Seixas De Melo, J.; Moura, A. P.; Melo, M. J. Photophysical and Spectroscopic Studies of Indigo Derivatives in Their Keto and Leuco Forms. *J. Phys. Chem. A* **2004**, *108*, 6975−6981.

(16) Iwakura, I.; Yabushita, A.; Kobayashi, T. Kinetic Isotope Effect on the Proton-Transfer in Indigo Carmine. *Chem. Phys. Lett.* **2010**, *484*, 354−357.

(17) Nagasawa, Y.; Taguri, R.; Matsuda, H.; Murakami, M.; Ohama, M.; Okada, T.; Miyasaka, H. The Effect of Hydrogen-Bonding on the Ultrafast Electronic Deactivation Dynamics of Indigo Carmine. *Phys. Chem. Chem. Phys.* **2004**, *6*, 5370−5378.

(18) Arsenault, E. A.; Yoneda, Y.; Iwai, M.; Niyogi, K. K.; Fleming, G. R. Vibronic Mixing Enables Ultrafast Energy Flow in Light-Harvesting Complex II. *Nat. Commun.* **2020**, *11*, 1460.

(19) Lewis, N. H. C.; Fleming, G. R. Two-Dimensional Electronic-Vibrational Spectroscopy of Chlorophyll *a* and *b*. *J. Phys. Chem. Lett.* **2016**, *7*, 831−837.

(20) Oliver, T. A. A.; Fleming, G. R. Following Coupled Electronic-Nuclear Motion through Conical Intersections in the Ultrafast Relaxation of *β*-Apo-8'-Carotenal. *J. Phys. Chem. B* **2015**, *119*, 11428.

(21) Oliver, T. A. A.; Lewis, N. H. C.; Fleming, G. R. Correlating the Motion of Electrons and Nuclei with Two-Dimensional Electronic-Vibrational Spectroscopy. *Proc. Natl. Acad. Sci. U. S. A.* **2014**, *111*, 10061−10066.

(22) Wu, E. C.; Arsenault, E. A.; Bhattacharyya, P.; Lewis, N. H. C.; Fleming, G. R. Two-Dimensional Electronic Vibrational Spectroscopy and Ultrafast Excitonic and Vibronic Photosynthetic Energy Transfer. *Faraday Discuss.* **2019**, *216*, 116−132.

(23) Lewis, N. H. C.; Dong, H.; Oliver, T. A. A.; Fleming, G. R. Measuring Correlated Electronic and Vibrational Spectral Dynamics Using Line Shapes in Two-Dimensional Electronic-Vibrational Spectroscopy. *J. Chem. Phys.* **2015**, *142*, 174202.
(24) Dong, H.; Lewis, N. H. C.; Oliver, T. A. A.; Fleming, G. R. Determining the Static Electronic and Vibrational Energy Correlations via Two-Dimensional Electronic-Vibrational Spectroscopy. *J. Chem. Phys.* **2015**, *142*, 174201.
(25) Wu, E. C.; Ge, Q.; Arsenault, E. A.; Lewis, N. H. C.; Gruenke, N. L.; Head-Gordon, M. J.; Fleming, G. R. Two-Dimensional Electronic-Vibrational Spectroscopic Study of Conical Intersection Dynamics: An Experimental and Electronic Structure Study. *Phys. Chem. Chem. Phys.* **2019**, *21*, 14153−14163.
(26) He, X.; Yu, P.; Zhao, J.; Wang, J. Efficient Vibrational Energy Transfer through Covalent Bond in Indigo Carmine Revealed by Nonlinear IR Spectroscopy. *J. Phys. Chem. B* **2017**, *121*, 9411−9421.
(27) Stephens, P. J.; Devlin, F. J.; Chabalowski, C. F.; Frisch, M. J. Ab Initio Calculation of Vibrational Absorption and Circular Dichroism Spectra Using Density Functional Force Fields. *J. Phys. Chem.* **1994**, *98*, 11623−11627.
(28) Becke, A. D. Density-Functional Thermochemistry. III. The Role of Exact Exchange. *J. Chem. Phys.* **1993**, *98*, 5648−5652.
(29) Frisch, M. J.; Pople, J. A.; Binkley, J. S. Self-Consistent Molecular Orbital Methods 25. Supplementary Functions for Gaussian Basis Sets. *J. Chem. Phys.* **1984**, *80*, 3265−3269.
(30) Cossi, M.; Rega, N.; Scalmani, G.; Barone, V. Energies, Structures, and Electronic Properties of Molecules in Solution with the C-PCM Solvation Model. *J. Comput. Chem.* **2003**, *24*, 669−681.
(31) Shao, Y.; Gan, Z.; Epifanovsky, E.; Gilbert, A. T. B.; Wormit, M.; Kussmann, J.; Lange, A. W.; Behn, A.; Deng, J.; Feng, X.; et al. Advances in Molecular Quantum Chemistry Contained in the Q-Chem 4 Program Package. *Mol. Phys.* **2015**, *113*, 184−215.
(32) Dreuw, A.; Head-Gordon, M. Single-Reference Ab Initio Methods for the Calculation of Excited States of Large Molecules. *Chem. Rev.* **2005**, *105*, 4009−4037.
(33) Li, T. C.; Tong, P. Q. Time-Dependent Density-Functional Theory for Multicomponent Systems. *Phys. Rev. A: At., Mol., Opt. Phys.* **1986**, *34*, 529−532.
(34) Lewis, N. H. C.; Dong, H.; Oliver, T. A. A.; Fleming, G. R. A Method for the Direct Measurement of Electronic Site Populations in a Molecular Aggregate Using Two-Dimensional Electronic-Vibrational Spectroscopy. *J. Chem. Phys.* **2015**, *143*, 124203.
(35) Zhang, X.; Herbert, J. M. Excited-State Deactivation Pathways in Uracil versus Hydrated Uracil: Solvatochromatic Shift in the 1$n\pi^*$ State Is the Key. *J. Phys. Chem. B* **2014**, *118*, 7806−7817.
(36) Maeda, S.; Ohno, K.; Morokuma, K. Updated Branching Plane for Finding Conical Intersections without Coupling Derivative Vectors. *J. Chem. Theory Comput.* **2010**, *6*, 1538−1545.
(37) Zhang, X.; Herbert, J. M. Analytic Derivative Couplings for Spin-Flip Configuration Interaction Singles and Spin-Flip Time-Dependent Density Functional Theory. *J. Chem. Phys.* **2014**, *141*, 064104.
(38) Becke, A. D. A. New Mixing of Hartree-Fock and Local Density-Functional Theories. *J. Chem. Phys.* **1993**, *98*, 1372−1377.
(39) Shao, Y.; Head-Gordon, M.; Krylov, A. I. The Spin-Flip Approach within Time-Dependent Density Functional Theory: Theory and Applications to Diradicals. *J. Chem. Phys.* **2003**, *118*, 4807−4818.
(40) Buenker, R. J.; Bonačić-Koutecký, V.; Pogliani, L. Potential Energy and Dipole Moment Surfaces for Simultaneous Torsion and Pyramidalization of Ethylene in Its Lowest-Lying Singlet Excited States: A Cl Study of the Sudden Polarization Effect. *J. Chem. Phys.* **1980**, *73*, 1836−1849.